Dependence of cooperative luminescence intensity on Yb^{3+} spatial distribution in crystals and glasses

P. Goldner,[1] B. Schaudel,[1,2] and M. Prassas[2]
[1]*Groupe Optique des Terres Rares, CNRS-UMR 7574, 1, Pl. A. Briand F-92190 Meudon, France*
[2]*Corning SA, Centre Européen de Recherche de Fontainebleau, 7 bis Av. de Valvins, F-77210 Avon, France*
(Received 6 August 2001; published 3 January 2002)

Cooperative emission has been recorded in several Yb^{3+} stoichiometric crystals. Its intensity, normalized by the square of the $^2F_{5/2}$ excited level population, is shown to depend only on the Yb^{3+} ions spatial distribution. In most cases, other material dependent parameters do not need to be taken into account, as confirmed by a theoretical analysis. Cooperative luminescence (CL) is therefore an easy way to probe Yb^{3+} clustering in crystals and glasses. This measurement has been carried out in aluminosilicate and phosphate glasses for which CL intensity strongly varies with the glass composition. Two models of Yb distribution are proposed to relate CL and glass structure or to allow easy comparison between samples. Finally, the extension of these results to other rare-earth ions and energy transfer processes is examined. It is found that dipole-dipole energy transfer and CL interaction coefficients vary in the same way but with reduced amplitude for the former. This results from the CL dependence on a quadrupole-dipole process at short distances.

DOI: 10.1103/PhysRevB.65.054103 PACS number(s): 78.55.−m, 78.20.−e, 42.70.Ce

I. INTRODUCTION

The spatial distribution of rare-earth ions (RE) has been largely studied in crystals and in glasses by optical spectroscopy. In the former, pairs or larger aggregates are often detected as minority sites exhibiting strong energy transfer, up conversion, or reduced lifetimes.[1–3] In some crystals such as $CsCdBr_3$, charge compensation favors RE pairs formation, which are then the main center and in which strong interactions are observed.[4,5] Even in lightly doped samples, where substitution of a trivalent cation is possible, it has been shown that pairs concentration can largely exceed that deduced from a statistical distribution.[6] In glasses, RE clustering has been also widely studied in the field of optical amplification.[7–9] The most common glass used in erbium doped fiber amplifiers, nearly pure silica, does not offer proper coordination spheres to RE. This explains the clusters which appear for RE concentrations above a few 100 ppm. In the case of erbium, a strong cross relaxation can occur between excited states of close ions leading to nonradiative deexcitation and to a decrease in the gain of the amplifier. To overcome this limitation, various synthesis methods have been developed[10] but the optimal Er^{3+} concentration for current amplifiers still remains under 500 ppm. Clustering has also to be avoided in the highly doped glasses which may be used for planar wave guides.

Quantitative characterization of RE clustering has been obtained mainly in fibers or guides by gain[10,11] or saturable absorption[12,13] measurements. In bulk samples, energy transfer probabilities can be determined but are not only related to RE distribution. Other parameters may have to be taken into account: phonon cutoff frequency for nonresonant transfer, lifetimes of acceptor's levels, and the absolute excited state density of the donor. In some cases, a complete analysis of the decay curve can bring information about RE-RE minimum distance.[14] NMR (Ref. 15) and extended x-ray absorption fine structure (EXAFS) (Ref. 16) may also be useful in determining RE distribution.

Yb^{3+} electronic configuration $4f^{13}$ is limited to two levels $^2F_{5/2}$ and $^2F_{7/2}$ separated approximately by 10 000 cm^{-1}. Yb^{3+} doped compounds emit visible light under infrared excitation in the $^2F_{7/2}\rightarrow{}^2F_{5/2}$ transition, around 1 μm. This fluorescence, which is centered at 500 nm, is known as cooperative luminescence (CL) and was first observed in $YbPO_4$.[17] It consists in the simultaneous deexcitation of two excited Yb^{3+} ions and the emission of one photon. The photon energy is then the sum of those of the two electronic transitions. The theory of cooperative absorption and emission, established by Dexter,[18] shows that an interaction between the two ions is necessary to observe the process. CL is therefore linked to the spatial distribution of Yb^{3+} ions and has been analyzed in this way in crystals and glasses.[19–24] Although cooperative emission, which is a second-order process, is very weak, it can be measured on bulk samples at relatively low excitation power densities.

In this paper, we first focus on the dependence of CL intensity on interionic distances in several stoichiometric crystals, to precise the effect of the parameters not related to distance. In a second part, an analysis is made of CL intensity variations in four oxide glasses and models are proposed to describe Yb^{3+} distribution. Finally, the possibility to transpose results obtained in Yb^{3+} doped samples to other RE is briefly examined.

II. EXPERIMENTS

Crystals were synthesized as polycrystalline powders by solid state reactions. Structures were checked by XRD. All glass samples were batch melt and details of the synthesis can be found elsewhere.[22] The molar composition of aluminosilicate glass (AS1, respectively, AS2) is SiO_2: 74% (62%), Na_2O: 20%, Al_2O_3: 6% (18%). They were prepared by Corning SA. P1 and P2 phosphate glasses have the general molar composition $(MgO\text{-}2Li_2O)_{1-x}(P_2O_5)_x$ with $x=0.8$ and 1.2 for P1 and P2. All glasses are doped with 5 % wt. Yb_2O_3.

CL was recorded through a Jobin-Yvon M25 monochromator equipped with a Hamamatsu H 6240-01 photon counting head. The excitation source was a Coherent S-98-1000C-100Q high power laser diode delivering approximately 400 mW at 975 nm. To ensure reproducibility, CL of glass samples was recorded on calibrated (≈ 80 μm) powders. Time resolved spectra and lifetimes were measured with a Hamamatsu InAs photodiode or a RCA photomultiplier and a pulsed BMI 802 pulsed Ti-Sa laser pumped by a BMI 520 YAG laser. Absorption and diffuse reflectance spectra were recorded on a Cary 17 spectrophotometer.

III. THEORY

A. Microscopic probability

Cooperative processes correspond to transitions simultaneously involving N ions and induced by Hamiltonians coupling M ions at a time with $M<N$. For example, cooperative sensitization is a three ions process due to Coulombic interaction $(N=3, M=2)$, whereas usual energy transfer involves only two ions $(N=2, M=2)$. In the case of cooperative luminescence (or absorption), transitions take place in two ions at the same time due to the one-center electromagnetic field-ion interaction. If the wave function ψ of the M ions system is simply written as the product of the individual wave functions $\psi=\Pi\psi_i$, the matrix elements between these states vanish since the ψ_i are orthogonal. Cooperative processes are allowed because of interactions between ions which prevent the separation of the M ions system wave function into one-ion wave functions.[18] In the case of CL, we consider two ions A and B with states ψ_a and ψ_b. The perturbed wave functions of the two-ions system are written as

$$\psi_{ab}=\psi_a\psi_b-\sum_{a',b'}\frac{\langle\psi_{a'}\psi_{b'}|H_{AB}|\psi_a\psi_b\rangle\psi_{a'}\psi_{b'}}{E_a+E_b-E_{a'}-E_{b'}}, \quad (1)$$

where H_{AB} is the interaction Hamiltonian and E_n the energy of state n. Electric dipole (*ed*) CL probability between pair states $|ab\rangle$ and $|a'b'\rangle$ for m polarization is then simply proportional to the matrix element

$$M_m=\langle ab|eD_m^{(1)}(A)+eD_m^{(1)}(B)|a'b'\rangle, \quad (2)$$

where $D_m^{(1)}$ is the usual one electron tensorial operator. Cooperative processes of higher order, such as magnetic dipole emission, are neglected since *ed* pair transitions are not forbidden in the case of Yb^{3+} ions.

Several interactions can result in CL but it has been shown[25] that multipolar electric processes are the largest for Yb^{3+}, allowing one to neglect magnetic and exchange mechanisms.

The electrostatic Hamiltonian is expressed as

$$H_{AB}=\sum_{i,j}\frac{e^2}{|r_i-r_j|},$$

where the sum runs over A and B electrons. In the case of nonoverlapping electronic wave functions, this Hamiltonian can be expanded using standard operator techniques and introduced in Eqs. (1) and (2). From this point the calculations can be performed using a number of approximations.[26] If the ions wave functions and positions are known, it is possible to compute cooperative transitions probabilities between Stark levels using only the closure procedure which is found in Judd's theory.[27] However, few crystal field analysis are available on Yb^{3+} ions and therefore the wave functions are generally unknown. To obtain manageable expressions, it is first of all necessary to average M_m versus the angular dependence on ions relative positions. Then several 3-j symbols have also to be averaged and finally a sum is performed over the Stark levels of each multiplet assuming equal populations of these levels. Finally, the only quantity which can be evaluated is the average value of $\Sigma_{a,b,a',b',m}M_m$. The validity of this calculation is discussed in Sec. IV C.

Under these assumptions, the largest emission probabilities are due to the quadrupole-dipole (*qd*) and forced dipole-dipole (fd-d) processes. The latter is not parity allowed but gains intensity from odd-parity configuration mixing. The relevant expressions are the following:[26,28]

$$\sum_{a,b,a',b'}\sum_m|M_m|^2=10\left(\frac{e^2}{R^4}\right)^2\Xi^2(1,2)\langle^2F_{5/2}\|U^{(2)}\|^2F_{7/2}\rangle^4\times\langle 4f\|r^2\|4f\rangle^2\langle f\|C^{(2)}\|f\rangle^2 \quad (3)$$

for the q-d process and

$$\sum_{a,b,a',b'}\sum_m|M_m|^2=\frac{20}{3}\left(\frac{e^2}{R^3}\right)^2\Xi^2(1,2)\langle^2F_{5/2}\|U^{(2)}\|^2F_{7/2}\rangle^2S(^2F_{5/2},^2F_{7/2}) \quad (4)$$

for the fd-d process. e is the electron charge (in ESU units), R the distance between the interacting ions, Ξ the closure factor defined by Judd, $U^{(k)}$ the reduced unit tensor operator and $C^{(k)}$ a reduced tensor operator related to the $Y_q^{(k)}$ spherical harmonics.[26] S is the line strength of the infrared transition $^2F_{7/2}\rightarrow{}^2F_{5/2}$.

The CL probability for two interacting ions is given by

$$K=\frac{64\pi^4e^2}{3h\lambda^3}\frac{n(n^2+2)^2}{9}\frac{1}{(2J+1)^2}\sum_{a,b,a',b'}\sum_m|M_m|^2, \quad (5)$$

where λ is the mean fluorescence wavelength (≈ 500 nm), n is the refraction index at λ and J is the total orbital quantum number of the emitting states $(J=\frac{5}{2})$. In the following, the dependence of K on interionic distance will be emphasized by using the reduced quantity (a/R) where a is a reference distance. In energy transfer studies, a critical distance is often defined as the one for which the transfer probability between two ions equals the isolated ions lifetime. However, CL probability is extremely weak compared to that of infrared deexcitation and there is little sense to define a similar critical distance. Since this study focuses on oxide compounds, a is chosen as the minimum Yb-Yb distance in

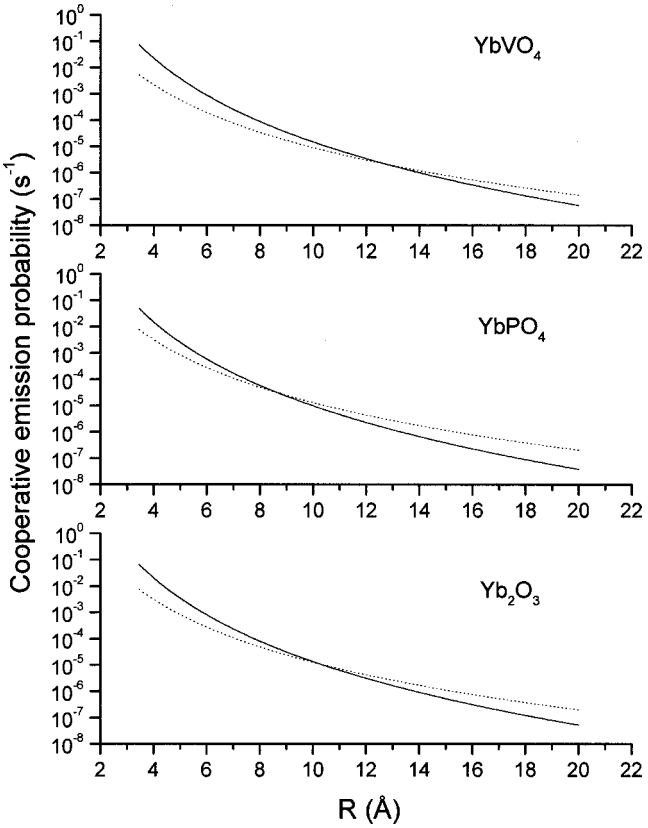

FIG. 1. Dependence of cooperative emission probability on distance R between interacting ions in Yb_2O_3, $YbPO_4$, and YVO_4. Solid line: quadrupole-dipole process, dotted line: forced dipole-dipole process.

Yb_2O_3 (3.45 Å) which is also likely to be the shortest distance found in an oxide glass. With our convention, Eq. (5) reads

$$K=K_{qd}(a)\left(\frac{a}{R}\right)^8+K_{fdd}(a)\left(\frac{a}{R}\right)^6 \tag{6}$$

for q-d and fd-d interactions. From Eqs. (3) and (4), the ratio K_{fdd}/K_{qd} is expressed as

$$\frac{K_{fdd}}{K_{qd}}=\frac{2Sa^2}{3\langle 4f\|r^2\|4f\rangle^2\langle f\|C^{(2)}\|f\rangle^2\langle {}^2F_{5/2}\|U^{(2)}\|^2F_{7/2}\rangle^2}. \tag{7}$$

K_{fdd}/K_{qd} depends mainly on S since the other parameters are usually considered as independent of the host. The radial and angular matrix elements are calculated from free ion wave functions[26] $\langle 4f\|r^2\|4f\rangle=0.691$ a.u., $\langle f\|C^{(2)}\|f\rangle^2=1.87$, and $\langle {}^2F_{5/2}\|U^{(2)}\|^2F_{7/2}\rangle=6/49$. S is calculated from ${}^2F_{5/2}$ radiative lifetime (see Sec. IV B).

The dependences on distance of the q-d and fd-d processes are shown on Fig. 1 with parameters corresponding to Yb_2O_3, $YbVO_4$, and $YbPO_4$ (Table I) and $\Xi(1,2)=9.5\times10^{-12}$ a.u./cm^{-1}.[26] For the three crystals, the calculated probabilities are lower than 0.1 s^{-1} even for very short distances between the interacting ions. The relative magnitude of q-d and fd-d processes change with values of S and the distances for which the two processes have equal probability are 8.7 Å for $YbPO_4$, 10.4 Å for Yb_2O_3, and 13.0 Å for $YbVO_4$. There is therefore a stronger variation on distance for short-range interaction.

B. Rate equation

Since the samples studied here have Yb^{3+} concentrations higher than 10^{20} cm^{-3}, a fast resonant nonradiative energy diffusion takes place. In this case, we simply write the evolution of Yb^{3+} levels populations using a rate equation

$$\frac{dN_1}{dt}=PN_0-\frac{N_1}{\tau}-\frac{X}{N_c}N_1^2, \tag{8}$$

where N_1 and N_0 are, respectively, the ${}^2F_{5/2}$ and ${}^2F_{7/2}$ level populations, P is the excitation rate, τ is the ${}^2F_{5/2}$ level lifetime, and N_c is the Yb^{3+} chemical concentration. X is the average cooperative interaction coefficient defined as

$$X=\overline{\sum_{n'}K(n,n')}, \tag{9}$$

where the sum runs over all neighbors n' of a given ion n. In the following, X will be evaluated for different materials and will be used to quantify Yb^{3+} clustering. Since CL probability is always very small compared to the infrared one at the excitation rates we used, the steady-state excited state population is simply given by

$$N_1\approx PN_0\tau.$$

For a sample of thickness e, the integrated CL intensity I_{coop} allowed us to calculate experimental values of X:

$$I_{\text{coop}}=\frac{1}{2}\int_0^e\frac{X}{N_c}N_1(z)^2dz=\frac{1}{2}\frac{X}{N_c}\tau^2I_{\text{laser}}^2\frac{\alpha}{2}(1-e^{-2\alpha e})$$

$$=\tau^2I_{\text{laser}}^2\frac{\alpha}{2}(1-e^{-2\alpha e})\int I_{\text{coop}}^N(\lambda)d\lambda, \tag{10}$$

where α is the absorption coefficient at the excitation wavelength and I_{laser} the excitation power density. $I_{\text{coop}}^N(\lambda)$ is the normalized CL. The thickness of the analyzed volume of powder has to be taken into account because it may not be optically thin, especially at high concentrations. To check the dependence of I_{coop} on α, CL excitation spectra were plotted versus absorption coefficient for several samples. Figure 2 shows excitation spectra of an aluminosilicate glass with absorption coefficients ranging from 0.4 to 8 cm^{-1} and of $YbPO_4$ which reaches 187 cm^{-1}. [The absorption coefficients of Yb:$LuPO_4$ (Ref. 29) were used for the latter compound]. The best fit of the experimental data of Fig. 2 by Eq. (10) corresponds to a thickness of 767 μm. It is worth noticing that Eq. (10) is able to describe the absorbed power on whole range of absorption.

Finally, it is important to clearly identify CL since pollution by other rare-earths ions can result in upconverted emissions by energy transfer in the same region.[22] The distinctive properties of the cooperative emission are first the absence of rise time under pulsed excitation (fast diffusion hypothesis).

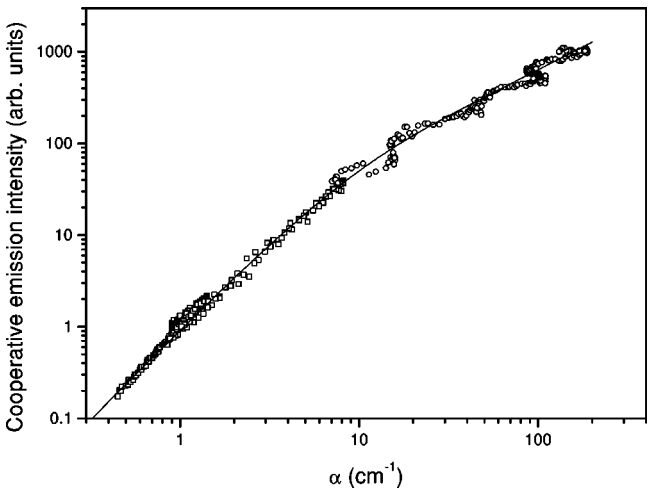

FIG. 2. Cooperative luminescence excitation spectrum versus absorption coefficient α in $YbPO_4$ (circles) and in a Yb^{3+} doped aluminosilicate glass (squares). Solid line: best fit according to Eq. (10) ($e=767\ \mu$m).

Upconversion by energy transfer involves intermediate levels and therefore always exhibits rise times. Excited state absorption should be negligible in Er^{3+} and Tm^{3+} ions which are the main impurities emitting in the 450–550 nm region. Second, the cooperative spectrum corresponds to the convolution of the infrared emission spectrum since energy is conserved. Most of the time, intensities are not always faithfully reproduced since CL probabilities are not directly linked to the infrared ones [see Eqs. (3) and (4)].

IV. COOPERATIVE EMISSION INTENSITY IN STOICHIOMETRIC CRYSTALS

To be able to quantify average cooperative interaction coefficient in a variety of materials, we have first calibrated our experiment with fully concentrated crystals (Yb_2O_3, $YbVO_4$, $YbPO_4$, and YbP_3O_9) in which Yb^{3+} ions positions are known. These crystals have been chosen to get significantly different ions distributions, allowing us to test Eqs. (3) and (4). In the following we first deal with the spectroscopic properties of these materials and then turn to quantitative analysis of CL intensities.

A. Spectroscopic properties

Figure 3 shows the visible emissions of Yb_2O_3, $YbPO_4$, $YbVO_4$, and YbP_3O_9 crystals. Convolutions of the IR spectra have been computed using the expression

$$f_{\mathrm{conv}}(E)=\int f_{\mathrm{IR}}(E')f_{\mathrm{IR}}(E-E')dE'$$

and are also plotted in comparison with the visible spectra. This allows us to clearly identify some impurities emissions (indicated by stars on the spectra), which we attribute to Er^{3+} and Tm^{3+} ions excited by Yb^{3+} through upconversion. However, as mentioned in the preceding section, the precise shape of the supposed cooperative emissions cannot be determined this way. Moreover, the contribution of the $^1G_4 \rightarrow {}^3H_6$ emission from Tm^{3+} (around 475 nm) to the band centered around 500 nm is difficult to estimate. We have therefore recorded time resolved spectra to separate cooperative lines from energy transfer related emissions by taking advantage of differences in rise times. Figure 4 shows the decay curves

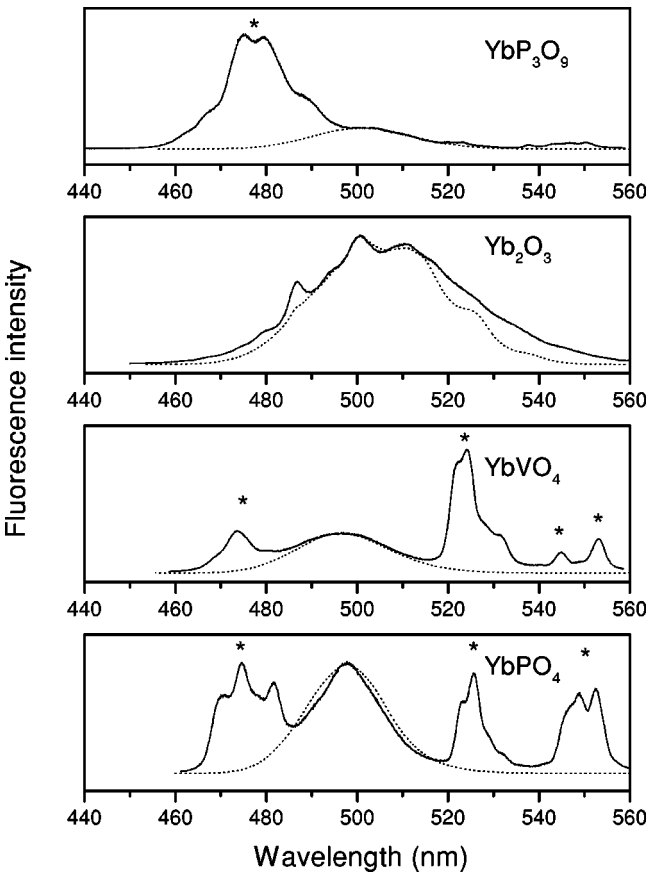

FIG. 3. Visible emissions of Yb_2O_3, $YbPO_4$, $YbVO_4$, and YbP_3O_9 under infrared excitation (975 nm). Dotted lines: convolution of IR spectrum. Stars denote emissions from Tm^{3+} and Er^{3+} impurities.

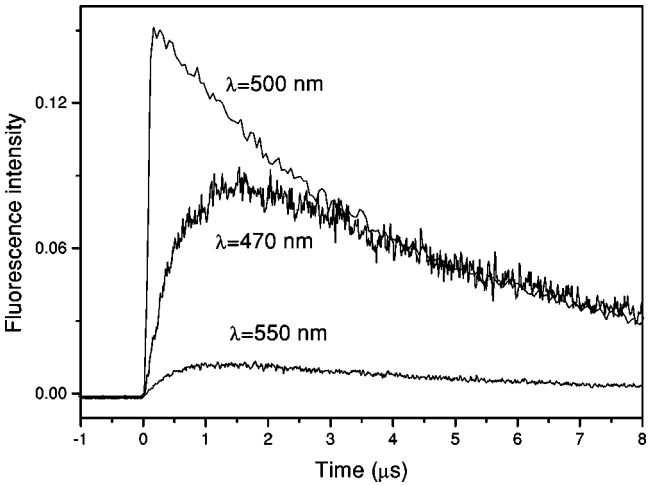

FIG. 4. Decay curves recorded at 500, 470, and 550 nm after excitation at 954 nm (pulse duration 8 ns) of $YbVO_4$.

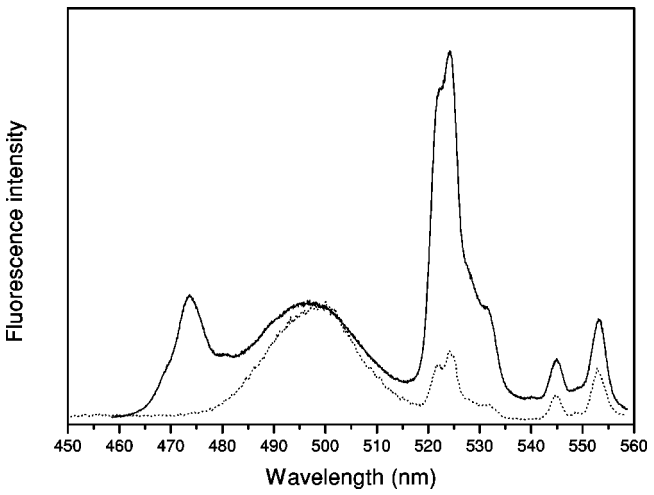

FIG. 5. Dotted line: time resolved emission spectrum (gate width: 200 ns, delay: 219 ns), solid line: emission spectrum under cw excitation.

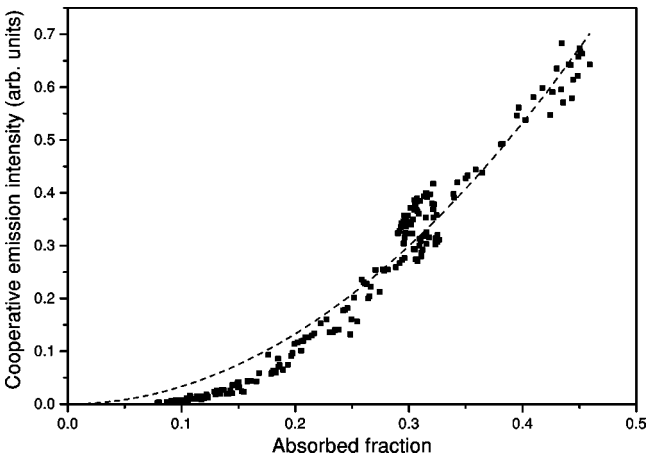

FIG. 6. Cooperative luminescence excitation spectrum versus absorbed fraction measured by diffuse reflectance in $YbPO_4$. Dashed line: quadratic fit.

recorded at 500, 470, and 550 nm in $YbVO_4$ using a short pulse excitation ($\approx$8 ns). The two latter emissions have respective rise times of 1.6 and 1 μs and reflect energy transfer mechanisms. On the opposite, the $\approx$100 ns rise time observed on the 500 nm decay is instrument limited, confirming the cooperative nature of this emission. A time resolved emission spectrum is shown in Fig. 5. The short delay after the excitation (219 ns) and the small width of the integration gate (200 ns) allows us to remove completely Tm^{3+} emissions and to strongly decrease Er^{3+} ones. (It was not possible, even for very small gates and delays, to obtain cooperative emission alone.) The spectra were normalized at 500 nm since decay curves show only cooperative process at this wavelength. CL actual shape is then easily found by deconvolution from the time-resolved spectrum. This procedure has been carried out for all the crystals prior to the integration of CL spectrum.

In order to evaluate the absorbed excitation powers in the different crystals, diffuse reflectance spectra were recorded and compared to cooperative luminescence excitation spectra. Figure 6 shows that, at high absorbed fractions coefficients, CL intensity depends quadratically on the absorbed power measured by diffuse reflection. This is not surprising since diffuse reflectance spectra saturate very easily at high absorption coefficients. The excitation wavelength used for cooperative intensity measurements (975 nm) lies well in the quadratic dependence region and we used this law for relative measurements between crystals. Infrared emission decay times are summarized in Table I.

B. Cooperative interaction coefficients

The structural data on the crystals studied are presented in Table I. The compounds were chosen to cover a wide range of cooperative interaction coefficients especially by varying the minimum distance between nearest neighbors. From the structures, we calculated for a given ion the sums $X_{th}/K_{qd} = \Sigma(a/R)^8 + (K_{fdd}/K_{qd})\Sigma(a/R)^6$ over all neighbors. The sums were then averaged according to the sites concentration. A large number of neighbors were taken into account to ensure convergence which occurred between $R_c = 6.55$ Å for the closely packed structure (Yb_2O_3) and $R_c = 13.98$ Å for large distances between ions (YbP_3O_9), as shown in Table I. R_c is the distance for which the sums reach 99% of their limit. To compute K_{fdd}/K_{qd}, S was determined from infrared lifetimes τ by the expression

$$S = \frac{3h(2J+1)\lambda^3}{64\pi^4 e^2 \chi \tau}.$$

These lifetimes, measured in lightly doped samples, were considered as radiative since Yb^{3+} is not very sensitive to nonradiative relaxation or concentration quenching. Magnetic dipole contributions to S are usually negligible. In the case of YbP_3O_9, no data on lifetimes were available, so that a range of values, representing approximately what is found in oxide crystals and glasses, is given. The ratios $K_{fdd}\Sigma(a/R)^6/K_{qd}\Sigma(a/R)^8$ are given in Table I. The fd-d contribution is higher in the larger structure YbP_3O_9, but the effect of S can be seen in the low value found for $YbVO_4$.

Experimental and theoretical values are shown in Fig. 7 and are in very good agreement on a large range (there is a factor of 50 between the highest and the lowest values for X). This suggests that, to a large extent, cooperative interaction coefficients depend mostly on the distance distribution between Yb^{3+} ions. An analysis of this result in the frame of the theory summarized in Sec. III is presented in the next section.

C. Discussion

A previous study on Yb:$CsCdBr_3$ single crystal showed that absolute values of cooperative luminescence intensities could be accounted for by multipolar interactions [Eqs. (3) and (4)] only within an order of magnitude.[25,28] However, Yb^{3+} spatial distribution (symmetric and asymmetric pairs) was not precisely known. In Yb:$LiNbO_3$, the same formula were used to deduce the ions pair concentration, which were in reasonable agreement with other experiments.[23] In both

TABLE I. Spectroscopic and structural parameters of Yb_2O_3, $YbPO_4$, $YbVO_4$, and YbP_3O_9.

Parameters	Yb_2O_3	$YbPO_4$	$YbVO_4$	YbP_3O_9
Space group	$Ia\bar{3}$	$I4_1/amd$	$I4_1/amd$	$P2_1/c$
Cell parameters (Å)	$a=10.434$	$a=b=6.816$ $c=5.966$	$a=b=7.043$ $c=6.247$	$a=11.219$ $b=19.983$ $c=9.999$ $\beta=97.3°$
Yb^{3+} concentration (cm^{-3})	2.82×10^{22}	1.44×10^{22}	1.29×10^{22}	5.4×10^{21}
Yb^{3+} sites and abundance	C_{3i}:0.25 C_2:0.75	D_{2d}	D_{2d}	C_i:2/12, C_i:2/12 C_1:4/12, C_1:4/12
R_c (Å)	6.55	9.06	9.16	13.98
Measured $^2F_{5/2}$ lifetime (μs)	18	48	40	100
Estimated radiative $^2F_{5/2}$ lifetime (ms)	0.85 (Ref. 40)	0.83 (Ref. 29)	1.2 (Ref. 41)	0.8–1.5
S (cm^2)	1.22×10^{-24}	1.72×10^{-24}	0.79×10^{-24}	$1.49–2.8\times10^{-24}$
Estimated refractive index	2.0 (Ref. 42)	1.83 (Ref. 29)	2.05	1.6 (Ref. 42)
$K_{fdd}\Sigma(a/R)^6/K_{qd}\Sigma(a/R)^8$	0.14	0.22	0.11	0.9–0.48
α (cm^{-1}) at 975 nm		187 (Ref. 29)		

cases, Eqs. (3) and (4), which contain no adjustable parameters, were found to give acceptable results, although several approximations are made in their derivations: (1) A closure procedure is performed, assuming completely degenerate configurations [$\Xi(1, 2)$ term], (2) populations of emitting level are equally distributed, (3) angular dependences are averaged.

The first two assumptions are used in the successful Judd-Ofelt theory,[27,30] although their validity can be questioned for some RE ions.[31] For Yb^{3+}, the energy differences between $4f$ and the exited configurations ($5d$ and ng) are large [$\Delta E(4f-5d)\approx100\,000\ cm^{-1}$] and is insensitive to the $4f$ energy range ($10\,000\ cm^{-1}$). On the other hand, the splitting of the $^2F_{7/2}$ and $^2F_{5/2}$ multiplets often reach 500–700 cm^{-1} which weakens the second hypothesis and restricts it at least to room temperature.

The angular average has also to be used carefully, especially with high symmetry sites. For example, electrostatic interactions between identical centrosymmetric sites vanish.[19] This has to be taken into account in compounds with single centrosymmetric sites, but when several sites exist, ions in centrosymmetric site have often most of their neighbors on different centrosymmetric and noncentrosymmetric sites. In the crystals studied here, only Yb_2O_3 and YbP_3O_9 have centrosymmetric sites (Table I). Removing interactions between identical centrosymmetric sites has little influence on average cooperative interaction coefficients. For example, $\Sigma(a/R)^8$ varies from 8.34 to 8.28 in Yb_2O_3 and 0.1140 to 0.1137 in YbP_3O_9. The other sites have rather low symmetries for which the averaging procedure should be more valid. Finally, the crystals chosen do not have low dimensionality which could strongly restrict RE relative positions. In glasses, RE sites have been shown to be of rather low symmetries (C_{2v}) (Ref. 32) and are disordered enough to provide accurate angular averaging.

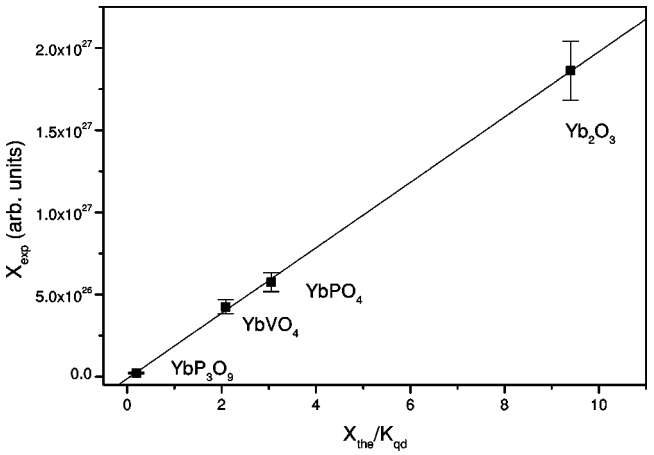

FIG. 7. Experimental (X_{exp}) average interaction coefficients plotted versus theoretical (X_{the}/K_{qd}) ones for several stoichiometric crystals (squares). Straight line: linear fit.

In summary, the approximations used to derive Eqs. (3) and (4) can be used in many hosts, although absolute values, computed with *ab initio* or measured parameters, may not reproduce accurately experimental results. It seems that a detailed study on a stoichiometric single crystal (such as Yb_2O_3) could be useful to completely check CL theory.

We now turn to the dependence of Eqs. (3) and (4) on the host material. The most sensitive (and unmeasurable) quantity is $\Xi(1,2)$ because it involves unshielded excited configurations. Limiting *nd* configurations to $5d$, $\Xi(1,2)$ is expressed as

$$\Xi(1,2)=2\left(-\frac{6\sqrt{14}}{35}\frac{\langle 4f|r|5d\rangle^2}{\Delta E(4f-5d)}-\frac{2\sqrt{14}}{21}\sum_n\frac{\langle 4f|r|ng\rangle\langle ng|r|4f\rangle}{\Delta E(4f-ng)}\right). \quad (11)$$

$\Xi(1,2)$ is also contained in the Ω_2 parameter of the Judd-Ofelt theory. Ω_2 has been shown to depend mostly on

crystal-field parameters and not on $5d$ electron density which modifies radial integrals. Only Ω_4 and Ω_6 show correlations with $5d$ electron density because they involve $\langle 4f|r^k|5d\rangle$ with $(k>2)$ integrals.[33] For fixed ion environment (i.e., constant crystal-field parameters), Ω_2 is well correlated to the covalency of the RE-ligand bond which is closely related to $\Delta E(4f-5d)$ (nephelauxetic effect).[34] $\Delta E(4f-5d)$ variation in oxide compounds can be estimated by the results of Dorenbos.[35] Applying his equations to Yb^{3+}, the lowest energy level of the $5d$ configuration is found between 51 340 and 72 340 cm^{-1} above the $4f$ configuration. This is only a 40% change for the whole range of oxide compounds. Since the barycenter of the $5d$ configuration is expected to vary much less than this (typically 3 to 4 times),[36] we can consider $\Delta E(4f-5d)$ as nearly constant for Yb^{3+} since our experimental errors are estimated to be $\pm 10\%$. Concerning ng configurations, the sum appearing in Eq. (11) can be evaluated by the closure procedure $\Sigma_n\langle 4f|r|ng\rangle\langle ng|r|ng\rangle \approx \langle 4f|r^2|4f\rangle$. Then, ng contribution to $\Xi(1,2)$ is 37% with $\Delta E(4f-ng)=217\,000\,cm^{-1}$. These configurations lie higher in energy than $5d$ and relative variations of $\Delta E(4f-ng)$ are also likely to be small.

In conclusion, the experimental result of Fig. 7, the dependence of X only on interionic distance, is in qualitative agreement with theory. Evaluating spatial distribution of Yb^{3+} ions by CL intensity, properly normalized, should be possible in a wide range of materials, although special cases of high symmetry sites have to be considered carefully. Parameters needed for normalization are easy to measure: $^2F_{5/2}$ lifetime and absorption coefficient at the excitation wavelength. This method can be also applied to other compounds, fluoride and bromides for example in which $\Delta E(4f-5d)$ is also fairly constant.[35] However in these low phonon materials, the weak CL is often hidden by emissions from Er^{3+} and Tm^{3+} ions excited by energy transfer upconversion. In this respect, purity of the samples is extremely important.

V. COOPERATIVE EMISSION IN YTTERBIUM DOPED GLASSES

A. Spectroscopic properties

Normalized CL spectra of aluminosilicate glasses AS1 and AS2 are shown in Fig. 8. The emission is centered around 500 nm with a spectral width of about 40 nm. AS2 has a much stronger CL than AS1 and in the latter case, upconverted emissions of Tm^{3+} and Er^{3+} which are present in the glass as impurities are clearly observed in the ranges 470–485 nm and 520–555 nm. The origin of the visible emission has been confirmed by convolution of the infrared emission spectrum and lifetimes measurements. For AS1, integrated CL intensity was determined by deconvoluting the emission spectrum and using CL spectrum free of impurities emission as a reference.

CL in phosphate glasses P1 and P2 is also centered around 500 nm (Fig. 9). However, its intensity is much lower than in AS glasses so that emissions of Tm^{3+} and Er^{3+} may be larger than CL if the purity of the samples (especially Yb_2O_3 starting material) is not high enough. As in AS1, careful deconvolution was performed to obtain reliable CL intensities.

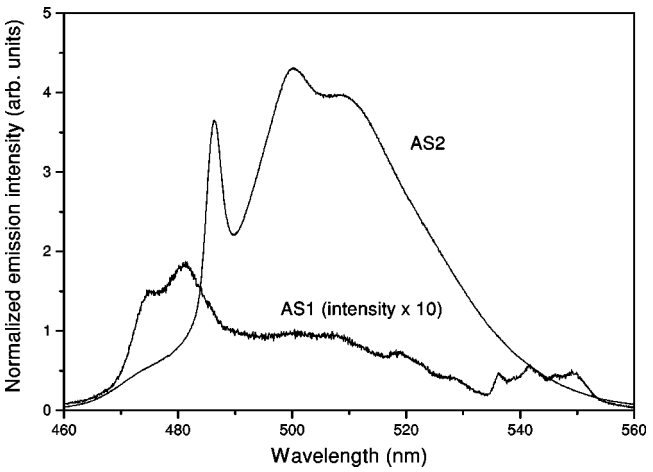

FIG. 8. Normalized cooperative emission spectra for aluminosilicate glasses AS1 and AS2.

B. Variation of the cooperative interaction coefficient

The cooperative interaction coefficient is determined in the same way for glasses as for stoichiometric crystals except that absorption coefficients could be measured and were used to directly normalize CL intensities. The parameters used in the calculations can be found in Table II. The values obtained are then compared to those found for $YbPO_4$, allowing us to determine X/X_{YbPO_4} for each sample (see Table II). Large variations of this ratio are observed in the silicate and phosphate glasses as their compositions vary. This effect is related to the structural changes of the glasses network.[22,37]

To get a more quantitative analysis of CL intensity variations, two models of Yb^{3+} distribution are proposed. They do not take into account the specific structures of each glass which define precisely the environment of RE ions and their spatial distribution. Such models, possibly determined from

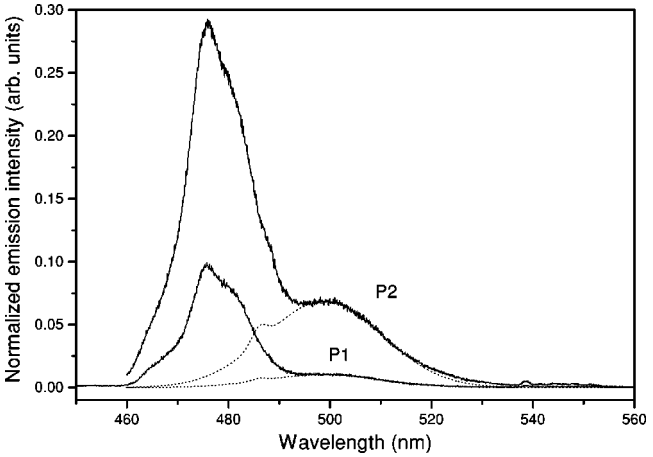

FIG. 9. Solid lines: Normalized visible emission spectra for phosphate glasses P1 and P2. Dotted lines: deconvoluted cooperative emission spectrum.

TABLE II. Spectroscopic data, cooperative luminescence and cross-relaxation average interaction coefficients and distribution parameters in Yb doped glasses.

Parameters	AS1	AS2	P1	P2
Yb^{3+} concentration (cm^{-3})	3.66×10^{20}	3.70×10^{20}	3.73×10^{20}	3.80×10^{20}
$^2F_{5/2}$ lifetime (ms)	1.90	1.0	1.0	1.0
refraction index	1.5	1.5	1.5	1.5
α (cm^{-1}) (at 975 nm)	1.49	4.83	3.07	3.47
X/X_{YbPO_4}	3.4×10^{-3}	0.15	5.86×10^{-4}	1.7×10^{-3}
X/X_{ref}	2.4	104.5	2.2	6.3
X_{CR}/X_{CRref}	1.5	31	1.4	2.6
d_0 (Å)	5.6	5.6	9.07	9.07
$f\times k$	0.03	1.91	0.02	0.1
N_{eff} (cm^{-3})	6.0×10^{19}	2.7×10^{21}	1.0×10^{19}	3.01×10^{19}
N_{eff}/N_c	0.16	7.2	2.7×10^{-2}	7.9×10^{-2}

molecular dynamics simulations, would be too complicated for a convenient treatment, especially in multicomponents glasses. In opposition, the following treatments are based on general reference distributions defined as random with a minimal distance between RE ions. The minimal distance requirement allows one to take into account the available ''sites'' for the RE ions. For a given concentration N_s of available sites, the random distribution is the limiting case of the quenching of an ideal melt if the RE concentration N_c is much lower than N_s.

In the first model, the chemical origin of the clustering is accounted for by dividing Yb^{3+} ions in two classes according to a characteristic distance d_0. Ions which have no neighbors within d_0 are considered to be ''homogeneously'' distributed and ions which have at least one neighbor within this distance are part of a cluster. In the latter, the minimum distance between two ions is a. Ions are randomly distributed in both classes since glasses usually do not restrict RE-RE distances to precise values. As seen in Sec. III A, this minimum distance is set to a, the shortest distance found in Yb_2O_3 ($a=3.45$ Å). The average cooperative interaction coefficient, resulting from the contributions of clusters and the homogeneous part, is given by

$$X=f\int_a^{d_0}4\pi R^2\frac{k}{V}\left[K_{qd}(a)\left(\frac{a}{R}\right)^8+K_{fdd}(a)\left(\frac{a}{R}\right)^6\right]dR,$$
$$+\int_{d_0}^{\infty}4\pi R^2N_c\left[K_{qd}(a)\left(\frac{a}{R}\right)^8+K_{fdd}(a)\left(\frac{a}{R}\right)^6\right]dR, \quad (12)$$

where $V=4/3\pi(d_0^3-a^3)$, $k+1$ is the average number of ions in the clusters, and f is the fraction of ions belonging to a cluster. This expression takes into account the fact that for a given ion, the contribution to X of its neighbors located at distances larger than d_0 is the same whether they belong to the homogeneous part or clusters. The clusters are also considered to be randomly distributed themselves.

In order to determine the last term of Eq. (12), a reference sample has to be chosen. Practically, a glass of close composition to those studied and having the lowest X is considered as free of clusters. In this case, $f=0$ and d_0 is calculated from the experimental value of X_{ref}. For all other samples with $X>X_{ref}$, the product fk is determined. Since we have access only to X, it is not possible to determine independently f and k. Figure 10 shows the f-k curves corresponding to AS1, AS2, P1, and P2 samples. For aluminosilicates (phosphates), the d_0 distance is 5.60 Å (9.07 Å), which is much lower than the highest minimal distance between ions at this concentration $d_{0,max}=2(3/4\pi N_c)^{1/3}\approx17$ Å. It can be seen that for high values of X, clusters must have a minimum size: in AS2, there is at least an average of 3.1 ions in each clusters. On the other extreme, it also possible that the sample contains larger clusters for lower f. As a limit for k, the case of Yb_2O_3 can be considered. For this crystal, each Yb^{3+} ion has about 19 neighbors within 5.6 Å. If such microcrystals exist in AS2, the corresponding fraction would be $f\approx0.1$.

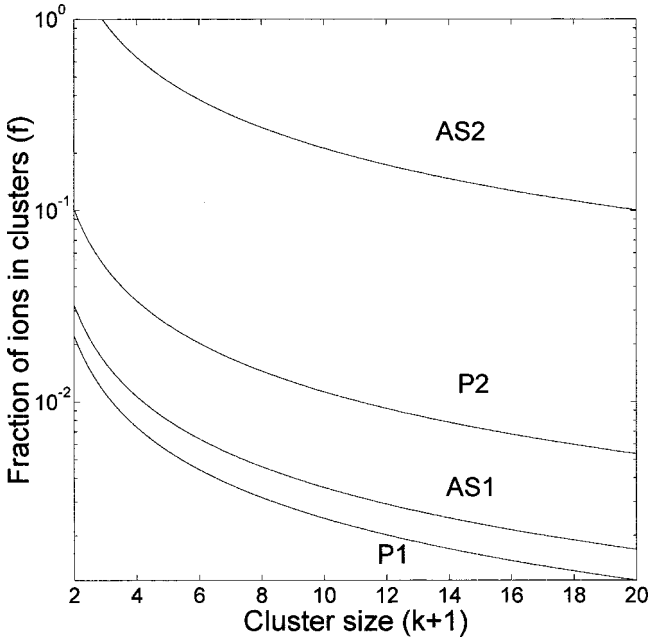

FIG. 10. Fraction of clusters versus cluster size in aluminosilicate and phosphate glasses.

On the other hand for glasses in which ions are well isolated from each other as in phosphate glasses, the *kf* product is always found to be very low, even if X vary significantly from one sample to the other. It may be useful then to keep only the homogeneous part of Eq. (12) and to calculate d_0 distances for each sample. For P1 and P2, this distance is 7.42 and 5.67 Å. The latter value compares well with the minimum distance of 5.6 Å between Nd^{3+} ions found in a glass of similar composition.[38]

This first model may be useful in comparing CL interaction coefficients with other measurements sensitive to clustering. However, each f-k curve is calculated relatively to a reference sample chosen in a given type of glass. This may lead to difficult comparisons: in Fig. 10, P2 appears as containing more clusters than AS1, although $X(\mathrm{AS1}) > X(\mathrm{P2})$. For the purpose of comparison between various kinds of glasses, a second description is therefore proposed.

In this model, the common reference for all materials with N_c RE concentration is the random distribution with a as the minimum distance between RE ions. The average interaction coefficient is given by

$$X_h(N_c) = \int_a^\infty 4\pi R^2 N_c \left[K_{qd}(a)\left(\frac{a}{R}\right)^8 + K_{fdd}(a)\left(\frac{a}{R}\right)^6 \right] dR. \tag{13}$$

Other samples may have, at the same concentration, higher or lower average interaction coefficients. In the first case, the sample will be considered as containing clusters and in the second case as being more homogeneous than the random distribution. Clusters are defined here in comparison with the random distribution and not with respect to the presence of close ions. An effective concentration is simply defined for any sample as

$$N_{\mathrm{eff}} = \frac{X}{X_h} N_c .$$

Values of N_{eff}/N_c of the glass samples are shown in Table II. For silicate glasses, it is possible to reach high values of clustering and it is interesting to compare the absolute values of N_{eff} with the concentrations of the crystals studied in Sec. IV. Even in the worst case, we reach $2.7\times10^{21}\,\mathrm{cm}^{-3}$, which is one order of magnitude lower than what is found in Yb_2O_3. Very high value of N_{eff} would indicate the formation of microcrystals. On the opposite, low N_{eff}, as in phosphate glasses, indicate interionic distances much larger than that of the random reference sample. The lower limit of the effective concentration, corresponding to $d_{0,\max}$, is $N_{\mathrm{eff}} \approx 5\times10^{17}\,\mathrm{cm}^{-3}$ which is still 20 times lower than N_{eff} for P1.

C. Extension to other rare-earth ions

The possible extension of the results obtained on Yb^{3+} to other RE assumes first that the spatial distribution is independent, to a reasonable extent, from the RE. This assumption should be quite justified for Tm^{3+} and Er^{3+} ions which sizes are close to Yb^{3+} one. Glasses may be also more suitable than crystals since the glass structure is often the most important parameter for RE distribution.[22] At low RE concentrations, the structure is unaffected by the doping. Another point to be considered is the nature of the interactions. Energy transfer, which is often the process of interest, can be due to a dipole-dipole mechanism which has R^{-6} dependence on RE-RE distance. Therefore variations of energy transfer average interaction coefficients may not follow CL ones.

As an example, an important and detrimental energy transfer, which is found in Er^{3+} doped fiber amplifiers, is the $(^4I_{13/2}, {}^4I_{13/2}) \rightarrow (^4I_{13/2}, {}^4I_{15/2})$ cross relaxation. This process reduces $^4I_{13/2}$ level population and the gain on the $^4I_{13/2} \rightarrow {}^4I_{15/2}$ transition at 1.55 μm. It is usually treated as a dipole-dipole mechanism with a critical distance of 1.0 nm in silicate glasses.[12,39] For highly doped glasses, fast resonant energy diffusion occurs and rate equations can be used in the same way as for CL (see Sec. III B). The average cross-relaxation probability X_{CR} is then expressed as

$$X_{\mathrm{CR}} = 0.5\left\{ f\int_a^{d_0} 4\pi R^2 \frac{k}{V}\left[K_{\mathrm{CR}}(a)\left(\frac{a}{R}\right)^6 \right] dR + \int_{d_0}^\infty 4\pi R^2 N_c \left[K_{\mathrm{CR}}(a)\left(\frac{a}{R}\right)^6 \right] dR \right\},$$

where K_{CR} is the probability of the cross relaxation between two ions at distance a. As in the case of CL, X_{CR} depends only on *fk* products. Assuming that K_{CR} does not vary in a type of glasses $X_{\mathrm{CR}}/X_{\mathrm{CRref}}$ ratios are presented in Table II for the four glasses studied above (the reference samples are those used in the CL study). Although qualitative variations are preserved, $X_{\mathrm{CR}}/X_{\mathrm{CRref}}$ ratios are 2–3 times smaller than X/X_{ref} as can be expected from the distance dependence of the processes. Since CL is dominated at short distances by a q-d process, the variations induced by clustering are more pronounced. Extension of CL results between materials of largely different compositions is also to be carefully performed since K_{CR} may be very dependent on parameters such as phonon cutoff frequency and overlap integrals.

VI. CONCLUSION

CL has been recorded in several Yb^{3+} stoichiometric crystals and its intensity was found to be well described by the sum of the two theoretically largest processes, quadrupole-dipole and dipole-dipole interactions. All parameters were kept constant except for the Yb-Yb distances distributions. This result shows that CL intensity, properly normalized by the square of the $^2F_{5/2}$ level population, can be easily used to quantitatively probe Yb^{3+} spatial distribution. This result is confirmed by an analysis of the microscopic CL emission probability. Due to the low multipolar order of interactions between Yb^{3+}, CL probability for a given Yb-Yb distance is related mainly to the energy difference between $4f^{13}$ and $5d4f^{12}$ configurations. Since the latter has limited evolution through the oxide compounds, we conclude that CL intensity is generally independent of the host for identical Yb distributions. However, in crystals where all RE sites symmetry is high or with low dimensional RE distributions, CL intensity may depart strongly from this conclusion.

RE clustering can be probed in glasses by CL measurements since RE sites symmetry are usually low and the random nature of the host increases the validity of the averaging used in CL probability calculations. Experiments are easier when RE impurities, especially Er and Tm, have low upconverted emissions. In low phonon or highly polluted materials, they may hide CL. Two models are proposed to analyze quantitatively CL intensity: in the first one clustering is defined with respect to the sample of close composition with the lowest CL intensity. This is useful, for example, to correlate clustering with glasses structures. To obtain a consistent parameter for comparing a wider range of materials, an effective concentration is defined using a reference random distribution with a minimal distance between ions corresponding to that found in Yb_2O_3 (3.45 Å). Finally, the results obtained with CL experiments can be transposed to energy transfer between other RE assuming identical distribution. When energy transfer probability is governed by dipole-dipole processes, its relative variations are lower than those of CL. For an accurate transposition, other parameters, such as phonon cutoff frequency and overlap integrals, have also to be taken into account.

ACKNOWLEDGMENTS

The authors thank F. Auzel for useful discussions and M. Genotelle for phosphate glasses synthesis.

[1] D. Tallant, M. Miller, and J. Wright, J. Chem. Phys. **65**, 510 (1976).
[2] R. Buisson and J. Vial, J. Phys. (France) **42**, L115 (1981).
[3] N. Pelletier-Allard and R. Pelletier, J. Phys. (France) **43**, 403 (1982).
[4] N. Cockroft, G. Jones, and D. N'Guyen, Phys. Rev. B **45**, 5187 (1992).
[5] F. Pellé and P. Goldner, Phys. Rev. B **48**, 9995 (1993).
[6] O. Guillot-Noël, V. Mehta, B. Viana, D. Gourier, M. Boukhris, and S. Jandl, Phys. Rev. B **61**, 15 338 (2000).
[7] K. Arai, H. Nakimawa, K. Kumata, T. Honda, Y. Ishii, and T. Handa, J. Appl. Phys. **59**, 3430 (1986).
[8] B. Ainslie, S. Craig, S. Davey, D. Barber, J. Taylor, and A. Gomes, J. Mater. Sci. Lett. **6**, 1361 (1987).
[9] B. Samson, L. Dong, J. de Sandro, and J. Caplen, Electron. Lett. **34**, 111 (1998).
[10] J. Wagener, P. Wysocki, M. Digonnet, and H. Shaw, Opt. Lett. **18**, 2014 (1993).
[11] J. Nilsson, B. Jaskorzynska, and P. Blixt, IEEE Photonics Technol. Lett. **5**, 1427 (1993).
[12] R. Quimby, W. Miniscalco, and B. Thomson, J. Appl. Phys. **76**, 4472 (1994).
[13] E. Maurice, G. Monnom, B. Dussardier, and D. Ostrowsky, Opt. Lett. **20**, 2487 (1995).
[14] T. Basiev, J. Phys. (Paris) **46**, C7 (1985).
[15] S. Sen and J. Stebbins, J. Non-Cryst. Solids **188**, 54 (1995).
[16] S. Sen, J. Non-Cryst. Solids **261**, 226 (2000).
[17] E. Nakazawa and S. Shionoya, Phys. Rev. Lett. **25**, 1710 (1970).
[18] D. Dexter, Phys. Rev. **126**, 1962 (1962).
[19] V. Ovsyankin, I. Podkolzina, and A. Fedorov, Izv. Akad. Nauk SSSR, Ser. Fiz. **43**, 1194 (1979).
[20] F. Auzel, D. Meichenin, F. Pellé, and P. Goldner, Opt. Mater. **4**, 35 (1994).
[21] F. Auzel, P. Goldner, and G. de Sa, J. Non-Cryst. Solids **265**, 185 (2000).
[22] B. Schaudel, P. Goldner, M. Prassas, and F. Auzel, J. Alloys Compd. **300-301**, 443 (2000).
[23] E. Montoya, L. Bausa, B. Schaudel, and P. Goldner, J. Chem. Phys. **114**, 3200 (2001).
[24] F. Auzel and P. Goldner, Opt. Mater. **16**, 93 (2001).
[25] P. Goldner, F. Pellé, and F. Auzel, J. Lumin. **72-74**, 901 (1997).
[26] T. Kushida, J. Phys. Soc. Jpn. **34**, 1318 (1973).
[27] B. Judd, Phys. Rev. **127**, 750 (1962).
[28] P. Goldner, F. Pellé, D. Meichenin, and F. Auzel, J. Lumin. **71**, 137 (1997).
[29] L. DeLoach, S. Payne, L. Chase, L. Smith, W. Kway, and W. Krupke, IEEE J. Quantum Electron. **29**, 1179 (1993).
[30] G. Ofelt, J. Chem. Phys. **37**, 511 (1962).
[31] R. Peacock, Struct. Bonding (Berlin) **22**, 83 (1975).
[32] T. Belliveau and D. Simkin, J. Non-Cryst. Solids **110**, 127 (1989).
[33] S. Tanabe, T. Ohyagi, N. Soga, and T. Hanada, Phys. Rev. B **46**, 3305 (1992).
[34] R. Reisfeld, Struct. Bonding (Berlin) **22**, 123 (1975).
[35] P. Dorenbos, J. Lumin. **91**, 155 (2000).
[36] P. Dorenbos, Phys. Rev. B **62**, 15 640 (2000).
[37] P. Goldner, B. Schaudel, M. Prassas, and F. Auzel, J. Lumin. **87–89**, 688 (2000).
[38] A. Avanesov, T. Basiev, Y. K. Voron'ko, B. Denker, A. Y. Karasik, G. Maksimova, V. Osiko, V. Pisarenko, and A. Prokhorov, Sov. Phys. JETP **50**, 886 (1979).
[39] J. Philipsen and A. Bjarklev, IEEE J. Quantum Electron. **QE-33**, 845 (1997).
[40] K. Petermann, G. Huber, L. Fornasiero, S. Kuch, E. Mix, V. Peters, and S. Basun, J. Lumin. **87–89**, 973 (2000).
[41] H. Xia, L. Li, H. Zhang, X. Meng, L. Zhu, Z. Yang, X. Liu, and Y. Wang, J. Appl. Phys. **87**, 269 (2000).
[42] A. Kaminskii, *Laser Crystals* (Springer-Verlag, Berlin, 1990).